GIS Odyssey Journal

2024 • Volume 4 • Number 1

https://doi.org/10.57599/gisoj.2024.4.1.5

Karol Dawidowicz[1]

PPP USING GALILEO-ONLY OBSERVATION IN RECEIVER ANTENNA PCC ASPECT

Abstract: Besides the Global Positioning System (GPS) and Globalnaya Navigatsionnaya Sputnikovaya Sistema (GLONASS), two additional global navigation satellite systems (GNSS) have reached full operational capability in recent years. The European Union, along with the European Space Agency, introduced the Galileo positioning system. China is developing the BeiDou system. To fully utilize the capabilities of the new systems, dedicated precise models and corrections are necessary. An example of such corrections can be antenna phase center corrections (PCC). In the case of Galileo, access to phase center corrections may be challenging. This is because a lot of GNSS antenna types still have no corrections directly dedicated to Galileo signals. In such a case, corrections created based on GPS signals are recommended. The study compared the positions of stations, determined based on Galileo-only observations using type-mean and individual PCC models obtained from field and anechoic chamber calibration. Additionally, calculations were performed using elevation-only PCC based on the type-mean model. It was demonstrated that position shifts resulting from the use of individual PCC derived from an out-door calibration instead of individual calibration in an anechoic chamber (dedicated PCC set for Galileo signals) can reach up to 5 mm in the vertical component, while for horizontal components, these shifts are generally less than 2 mm.

Keywords: phase center corrections (PCC), Galileo, precise point positioning (PPP)

Received: 12 April 2024; accepted: 14 May 2024

[1] University of Warmia and Mazury, Faculty of Geoengineering, Department of Geodesy, Olsztyn, ORCID ID: http://orcid.org/0000-0002-8837-700X, email: karol.dawidowicz@uwm.edu.pl

Introduction

Today's satellite systems were initiated by the Transit system, created in 1958 at the Applied Physics Laboratory of Johns Hopkins University in the USA. Initially designed for military purposes, the system quickly found practical applications in marine navigation and served as a geodetic aid and frequency standard source. As of December 31, 1996, it was transformed into the Global Positioning System (GPS), which was designed as a precise global positioning system. Apart from GPS, we can distinguish several other global satellite systems. GLONASS (Globalnaya Navigatsionnaya Sputnikovaya Sistema) is the Russian counterpart of GPS. Galileo is the European satellite navigation system, officially launched on December 15, 2016. BeiDou is the Chinese satellite navigation system, which initially covered only the region of China and neighbouring countries, but now its coverage has been extended globally.
In addition to introducing new systems, existing first-generation satellite navigation systems are evolving into new, modernized forms. Modernized GPS and GLONASS systems bring, among other things, new signals. Modern GNSS satellites will emit at least three civil signals across multiple frequency bands.

New satellites and new signals present a tremendous opportunity for GNSS receivers to achieve greater resistance to interference and bigger accuracy. There are many potential benefits of multi-GNSS applications:

- achieving high positioning accuracy with an increased number of satellites,
- improving positioning effectiveness by receiving a significantly larger number of satellite signals, even in challenging conditions (urban canyons, etc.),
- increasing resistance to interference by utilizing different frequency bands.

Galileo – the European satellite navigation system is an equivalent alternative to the American GPS, Russian GLONASS, and Chinese BeiDou systems, but unlike them, it is controlled by civilian institutions. Its advantage and reason for being a competitor and complement to GPS is its smaller margin of error (ultimately expected to be around 1 m on the open frequency and about 10 cm on the paid frequency).
The space segment consists of 24 operational satellites and 6 backups, evenly distributed across three orbits. The orbit altitude is 23,222 km, with an inclination angle of 56°. Satellites broadcast signals in three frequency bands (Bartolomé et al., 2014).
The control system for Galileo consists of two independent segments: the Ground Control System (GCS), responsible for monitoring the technical status of satellites and filling gaps in satellite configuration, and the Ground Mission System (GMS), responsible for overall system operation control. The GCS segment includes five control stations providing continuous monitoring and two-way communication with all system satellites. The GSS segment is composed of several Ground Sensor Stations (GSS) distributed worldwide, allowing for continuous monitoring of all satellites. Collected data is transmitted to the Galileo Control Center (GCC), where analysis is performed, and based on this, a navigation dispatch is generated and sent to satellites via 10 Up-Link Stations (ULS).

The methodology of GNSS antenna calibration has been developing since the 1980s. These methods can generally be divided into absolute and relative, or field and laboratory procedures (Zeimetz & Kuhlmann, 2008). Relative Phase Center Corrections (PCCs) are estimated when the phase center position of the calibrated GNSS antenna is determined relative to a reference antenna (usually a Dorne Margolin T antenna, assuming the phase center variation of the reference antenna is zero). Absolute methods are referred to when PCCs are determined independently of a reference antenna. Field procedures are based on tracking actual satellite signals (Wubbena et al., 2000, Bilich & Mader, 2010), while laboratory procedures are conducted in an anechoic chamber and utilize simulated (artificial) GNSS signals (Gorres et al., 2006).

In addition to the classification based on the calibration method, PCC models are divided into individual and type-mean. An individual antenna PCC model is created when a specific antenna unit, along with its radome, is calibrated. In mean calibration, several antennas of the same type are calibrated, and the final PCC model is created by combining all the results into a single file.

So far, GNSS antenna models have been created using field calibration only for the two frequencies of the GPS and GLONASS signals. Meanwhile, modernized GPS and GLONASS systems transmit new signals using new carrier frequencies. Additionally, the development of new satellite systems, such as Galileo and BeiDou, necessitates their inclusion in the antenna calibration procedure.

Only a few centers worldwide are involved in GNSS antenna calibration. In recent years, Geoscience Australia has become one of these facilities, the only one in the Southern Hemisphere (Riddell et al., 2015). Previously active centers include the National Geodetic Survey (Virginia, USA), the University of Bonn (Bonn, Germany), SenB (Berlin, Germany), Geo++ (Hannover, Germany), and the Institute of Geodesy (IfE) (Hannover, Germany). Recently, the first calibration results for antennas obtained at Wuhan University (Hu et al., 2015) and ETH Zurich (Willi et al., 2018) have also been published. Calibration systems are also being developed at UWM Olsztyn (Dawidowicz et al., 2021) and the University of Zagreb (Tupek et al., 2023). Despite the significant increase in the number of GNSS antenna calibration centers, access to phase center corrections may be challenging. This is due to a large number of GNSS antenna types, and the calibration process itself is time and money-consuming. Therefore, in the absence of corrections specifically dedicated to Galileo signals, it is recommended to use corrections created based on GPS signals. Additionally, the issue is complicated because depending on the calibration method, GNSS antenna PCCs may differ by several millimeters (Bilich & Mader, 2010; Baire et al., 2013; Dawidowicz & Krzan 2016; Krzan et al., 2020). In the work of Bilich & Mader (2010), for example, the results of absolute calibration provided by three calibration centers (two in the field and one in an anechoic chamber: Geo++, NGS, and the University of Bonn) were compared. The results showed that differences in PCCs can reach up to 5 mm for corrections at low elevations (up to 20°). These differences significantly increase when creating linear combinations of signals.

The study compared station positions determined based on Galileo-only observations using type-mean calibration models and individual models obtained from

calibration in an anechoic chamber and outdoors. Additionally, to estimate the impact of simplifications in calibration models on position components, calculations were performed using elevation-only PCCs separated from the type-mean model. The main motivation of the study was to estimate the differences in position components resulting from using different PCC models in processing Galileo-only observations.

Methodology

The analysis is based on multi-frequency Galileo system observations recorded at ten selected EPN stations (Fig. 1) from January 1st to January 10th, 2021.

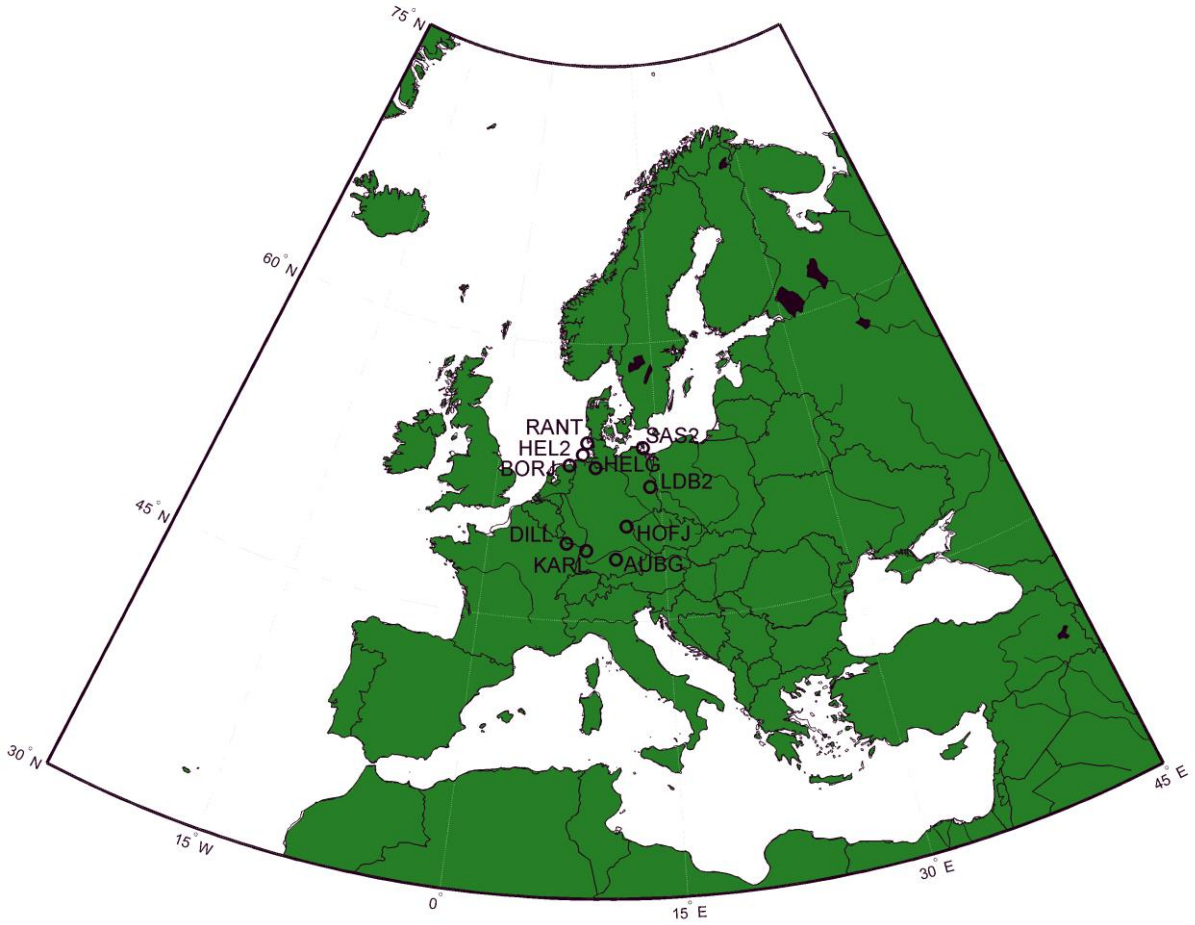

Fig. 1. Geographical location of the stations
Source: own study

Daily observations were divided into 30-minute observation windows, resulting in 480 half-hour sessions for each station. Observing was processed using the open-source GAMP software package (Zhou et al., 2018). The equipment placed at the selected stations is presented in Table 1.

Table 1. Stations' hardware

Site	Receiver	Antenna
AUBG	LEICA GR50	LEIAR25.R4 LEIT
BORJ	JAVAD TRE_3 DELTA	LEIAR25.R4 LEIT
DILL	LEICA GR50	LEIAR25.R4 LEIT
HEL2	LEICA GR50	LEIAR25.R4 LEIT
HELG	JAVAD TRE_3 DELTA	LEIAR25.R4 LEIT
HOFJ	LEICA GR50	LEIAR25.R4 LEIT
KARL	JAVAD TRE_3 DELTA	LEIAR25.R4 LEIT
LDB2	LEICA GR50	LEIAR25.R4 LEIT
RANT	JAVAD TRE_3 DELTA	LEIAR25.R4 LEIT
SAS2	JAVAD TRE_3 DELTA	LEIAR25.R4 LEIT

Source: own study

The observations were processed using type-mean PCC (igs14_2035.atx) recommended by IGS and individual PCC models recommended for use in the EPN network. Since all selected stations had both types of individual models (obtained from calibration in an anechoic chamber and outdoor calibration using a robot), both possible variants were considered in the analyses (columns 3 and 4 in Table 2: where in the .atx file name, the first four digits denote the year, the next two denote the month, and the following two denote the day of calibration). Additionally, for the purposes of analysis, calculations were made using only elevation-only PCC obtained from the igs14_2035.atx model (Table 2).

Table 2. PCC models used

Site	Type-mean (14)	Type-mean elevation-only (14e)	Individual robot-derived (i.r.)	Individual chamber-derived (i.c.)
	1	2	3	4
AUBG	igs14_2035.atx	igs14_2035_eo.atx	20130111.atx	20180823.atx
BORJ			20160707.atx	20171013.atx
DILL			20110725.atx	20110913.atx
HEL2			20141117.atx	20180425.atx
HELG			20160406.atx	20180424.atx
HOFJ			20120924.atx	20180823.atx
KARL			20110729.atx	20110912.atx
LDB2			20190613.atx	20190520.atx
RANT			20110708.atx	20190118.atx
SAS2			20100907.atx	20190319.atx

Source: own study

Notably, for the type-mean and individual models from field calibration, the PCC files contain corrections only for observations on frequencies L1 and L2 for GPS and

GLONASS signals. In the case of calibration in an anechoic chamber, the PCC files contain corrections for observations on all frequencies used in the Galileo system. Processing the proposed variants will result in solutions using outdoor derived models (type-mean, type-mean elevation only, and individual robot); PCC corrections will be adopted from the GPS system. Conversely, in the case of solutions using individual models developed in an anechoic chamber, observations will be improved based on dedicated corrections.
The open-source software GAMP was used to process GNSS observations. GAMP is a program based on RTKLib but includes enhancements such as cycle slip detection, receiver clock jump repair, and handling of GLONASS inter-frequency errors. The characteristics of the software and its capabilities are presented in (Zhou et al., 2018). The main parameters adopted for processing observations using the GAMP are presented in Table 3.

Table 3. GAMP processing parameters

Basic observables	Undifferenced carrier phase & pseudorange;
Orbit & clock products	CODE MGEX orbits and clocks;
Ionospheric delay	The undifferenced and uncombined (UC) dual-frequency observations were used in PPP processing to extract ionospheric delays and avoid noise amplification (Pengfei et al., 2011);
Tropospheric delay	Zenith dry delay estimated as a parameter; Wet delay estimated using the wet GMF mapping function;
Ocean loadings	FES2004 model using ONSALA ocean loading service (Lyard et al., 2006);
Differential Code Biases	Daily multi-GNSS differential code biases (DCBs) are derived from observations of MGEX/iGMAS networks with local ionospheric TEC modeling technique entitled MGTS. A description of MGTS algorithms is provided in Wang et al. (2016)
Other	Observation sampling rate: 30 sec.; Elevation angle cut-off 10°; Daily observations from the period 01.01.2021-10.01.2021; Ambiguity float solution

Source: own study

PCC comparison

Previous studies on the impact of PCC models on positioning have indicated that transitions between different types of correction models, such as from relative to absolute or from mean to individual, result in noticeable changes in position components (Baire et al. 2013, Dawidowicz and Krzan 2016) obtained from GPS, GLONASS, or GPS+GLONASS processing. Another problem may be the lack of dedicated

corrections for SVs of new systems' signals (e.g., Galileo) and the adoption of them from existing ones. This study focuses on this issue.

In the chapter, the differences between various PCC models were analyzed. Fig. 2 illustrates the differences determined based on elevation-only PCC data calculated for all analyzed stations. For the purpose of this comparison, type-mean PCCs obtained from the igs14_2035.atx model as well as both individual models were converted to a common PCO (obtained from the type-mean model), and then differences in PCC were calculated and presented. The conversion to a common phase center was performed using the approach proposed by Schön and Kersten (2013).

First, both sets of PCVs must be shifted to a common reference, where PCV(α,0) = 0 (zenith PCV = 0). This shift is performed by adding a constant value δ = -PCV(α,0) to all derived PCVs. As a result of this step, the vertical component of PCO should also be corrected. Such correction is made using the following formula: $PCOup^{corr}$=PCOup-δ. In the final step, the reduced corrections are calculated using the formula:

$$PCC(\alpha, z) = s^T PCO_r + \left(PCV_c(\alpha, z) + s^T (PCO_c - PCO_r)\right) \qquad (1)$$

where PCC denotes the compared PCC after reduction to reference PCO, PCOr is the PCO of the reference model, PCVc denotes the PCV of the compared model, and PCOc is the PCO of the compared model.

The reduced corrections obtained in this way can be used to create difference patterns (dPCCs). Fig. 2 illustrates elevation-only differences in PCCs (dPCCs) between the igs14.atx model and two individual models at 10 stations used for analysis, calculated for frequencies L1, L2, and their linear combination IF, for Galileo system signals. For Galileo observations in solutions using outdoor-derived models (type-mean or individual), PCC corrections were adopted from the GPS system. On the other hand, dedicated corrections were used for the analysis for solutions using individual models elaborated in an anechoic chamber.

Analyzing the differences presented in Fig. 2, we can observe that for the L1 frequency, the results are the smallest and generally do not exceed 2 mm. Exceptions are stations HOFJ and HEL2 where differences are larger, reaching up to 4 mm. As expected, the differences between the type-mean and individual models calibrated out-door with a robot are the smallest. This is due to the fact that the models were developed using the same calibration technique.

For the L2/L5 frequencies, the differences are noticeably larger: in most cases, they exceed 5 mm. An exception is again the comparison of models from field calibration, where differences generally do not exceed 2 mm. Comparing the curves for individual stations, their similarity can be observed. Visible deviations only concern station LDB2, where the curve differs significantly, and additionally, the differences resulting from the comparison of two models from field calibration reach up to 5 mm.

The differences obtained for the IF linear combination are significantly larger and exceed 10 mm in the case of comparing models obtained from field calibration and calibration in an anechoic chamber.

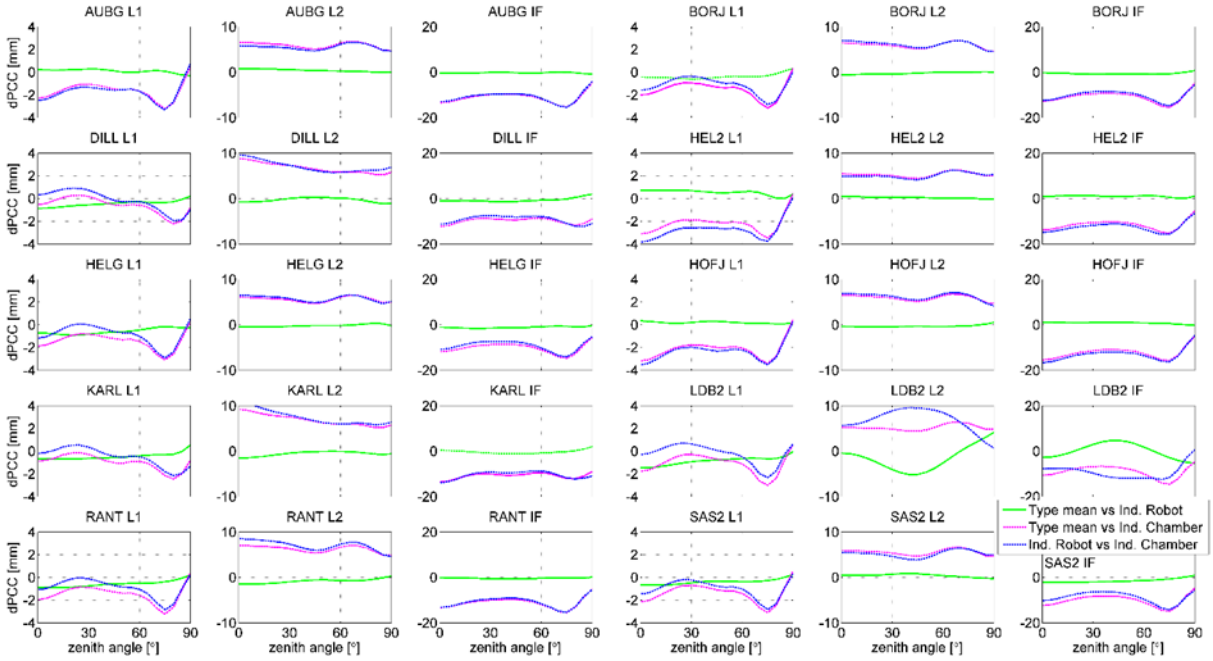

Fig. 2. Elevation-only PCC differences
Source: own study

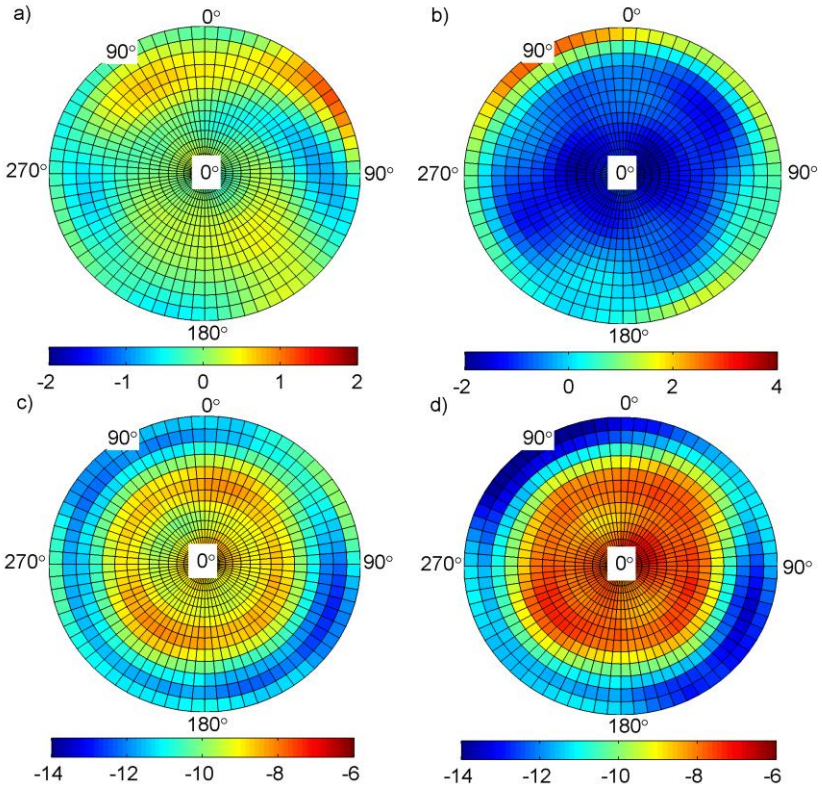

Fig. 3. Full PCC differences for DILL station: a) igs14-igs14 elevation only, b) igs14-individual robot, c) igs14-individual chamber, d) individual robot-individual chamber
Source: own study

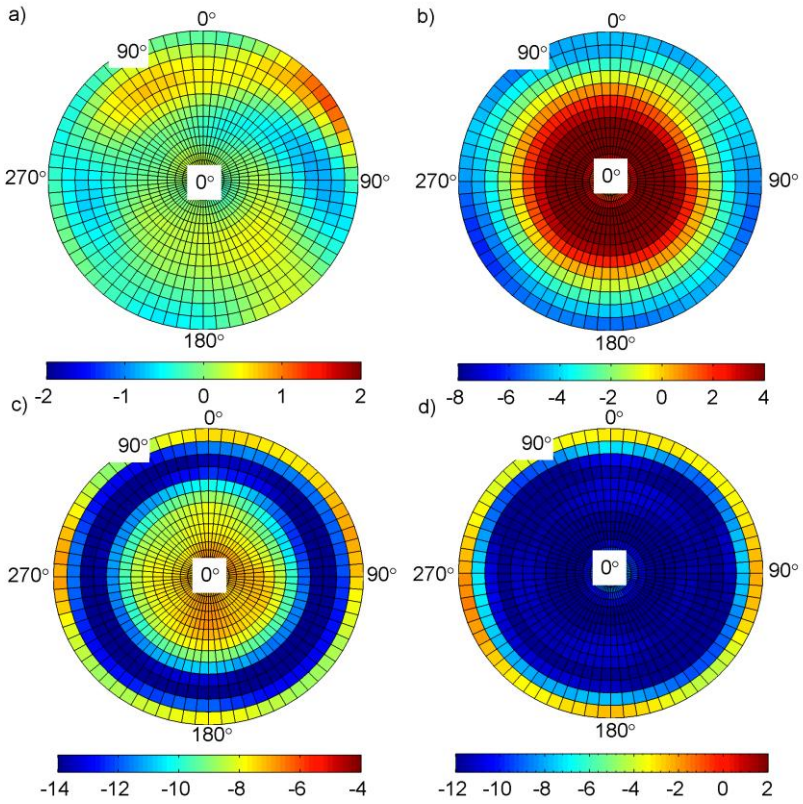

Fig. 4. Full PCC differences for LDB2 station: a) igs14-igs14 elevation only, b) igs14-individual robot, c) igs14-individual chamber, d) individual robot-individual chamber
Source: own study

In Figs 3 and 4, full dPCCs for selected two stations (DILL and LDB2) are presented, including comparisons with elevation-only models. The smallest differences were obtained when comparing full models with elevation-only models (a). In the case of both stations, the differences for these two comparisons do not exceed 2 mm in any antenna area. Small differences were expected, as elevation-only models can be considered a first approximation of full models. Elevation-only models are still used in some older versions of software. Slightly larger differences were obtained for the comparison of the type-mean model and the individual model from field calibration. In the case of both stations, the differences for this comparison exceed 3 mm in some antenna areas, especially for high zenith angles. The largest differences were obtained for the comparison of the chamber model with two models derived from field calibration. These differences reach up to 15 mm in some areas of both antennas. The reasons for such large differences should be attributed to significant differences in the Up component of PCO, which additionally accumulate during the creation of IF combinations. The up component of PCO for both compared antennas is presented in Table 4.

Table 4. PCO comparison

Site	Up of PCO [mm]			ΔUp of PCO [mm]		
	type-mean	rob. ind.	cham. ind.	1-2	1-3	2-3
	1	2	3			
DILL L1	159.13	158.26	156.53	0.87	2.6	1.73
DILL L2	154.84	154.06	165.21	0.78	-10.37	-11.15
LDB2 L1	159.13	157.65	154.95	1.48	4.18	2.7
LDB2 L2	154.84	159.34	162.67	-4.5	-7.83	-3.33

Source: own study

Results

This part of the work presents differences from comparing position components determined using individual antenna PCC models, the type-mean model (igs14.atx), and the so-called elevation-only model derived from igs14.atx. Thirty-minute observation windows were used to study short-period oscillations.

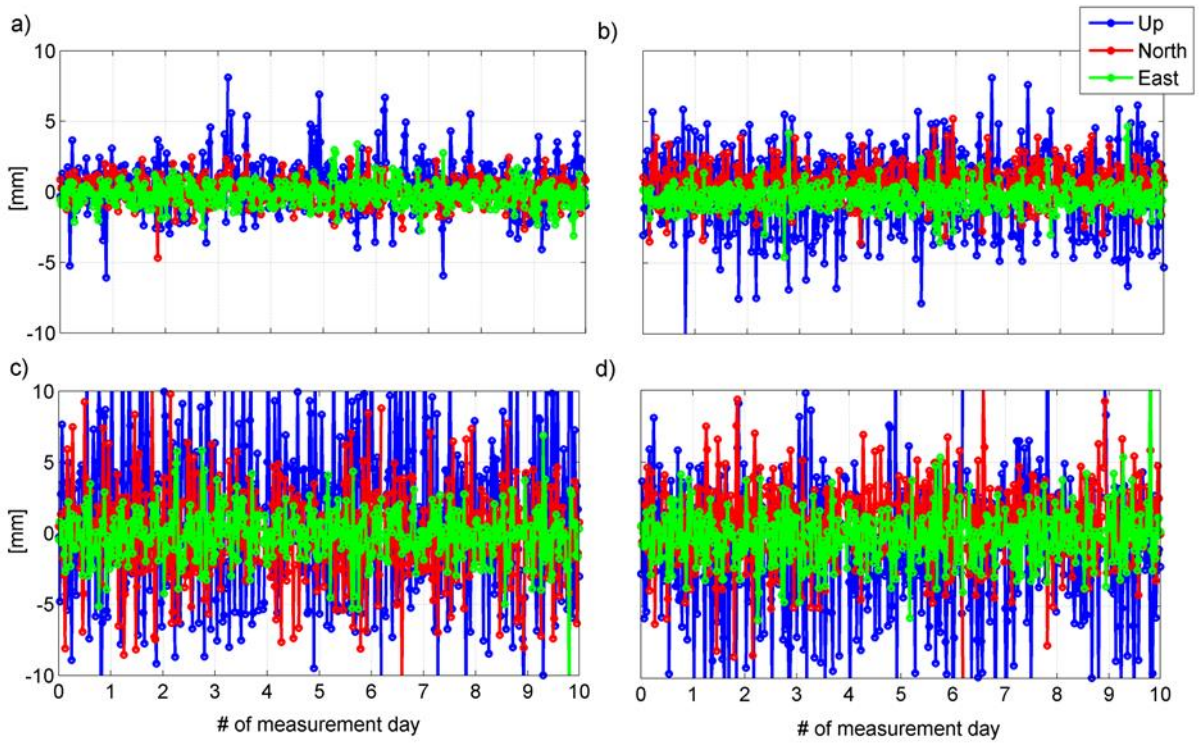

Fig. 5. Time series of differences for DILL station from 0.5-hour observation window a) igs14 elevation-only vs igs14; b) individual robot vs igs14; c) individual chamber vs igs14; d) individual robot vs individual chamber

Source: own study

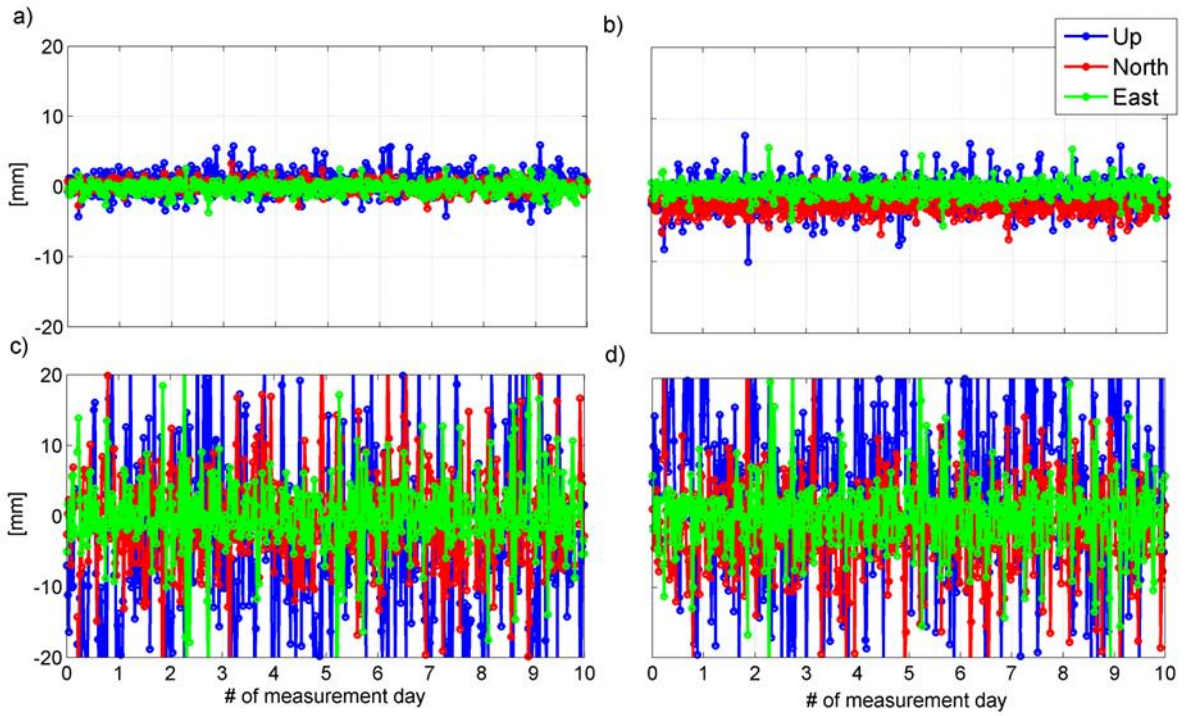

Fig. 6. TS of differences for LDB2 station from 0.5-hour observation window: a) igs14 elevation-only vs igs14; b) individual robot vs igs14; c) individual chamber vs igs14; d) individual robot vs individual chamber
Source: own study

All observations were processed using the "free network" method in the IGb08 system (aligned with the International Terrestrial Reference Frame 2008 (ITRF2008)). Since the analysis of time series mainly concerns topocentric coordinates (horizontal components N, E, and vertical component U), the obtained time series were converted to the topocentric system. For the sake of clarity in the presentation, detailed analyses and results are provided only for selected 2 stations (DILL and LDB2). Figs 5 and 6 illustrate coordinate time series differences (dNdEdU) for example dPCC models.

Analyzing the obtained differences for all three position components, it can be observed that the results have similar magnitudes and trends regardless of the station. In all cases, it can be observed that the differences for the horizontal components are smaller than the differences obtained for the vertical component. Maximum differences for the vertical component exceed 20 mm (station LDB2: comparison of two individual models), while for the horizontal components, they do not exceed 15 mm (same solution).

Additionally, it can be observed that the differences obtained in comparisons of solutions obtained using models derived from chamber and robot calibration exhibit the largest spread. In the case of both stations, these differences exceed 10 mm. In the case of the other two comparisons (where robot-derived PCC models were used), the differences are evidently smaller and generally do not exceed 5 mm.

For station LDB2, the analyzed differences are slightly larger, which may be due to larger differences observed in the used PCC models for this station (compared to station DILL). As expected, the smallest differences were obtained when comparing the type-mean and type-mean elevation-only models.

Figs 7 and 8 depict the mean differences obtained from daily and 0.5-hourly solutions for all possible variants, along with their corresponding standard deviations (STD).

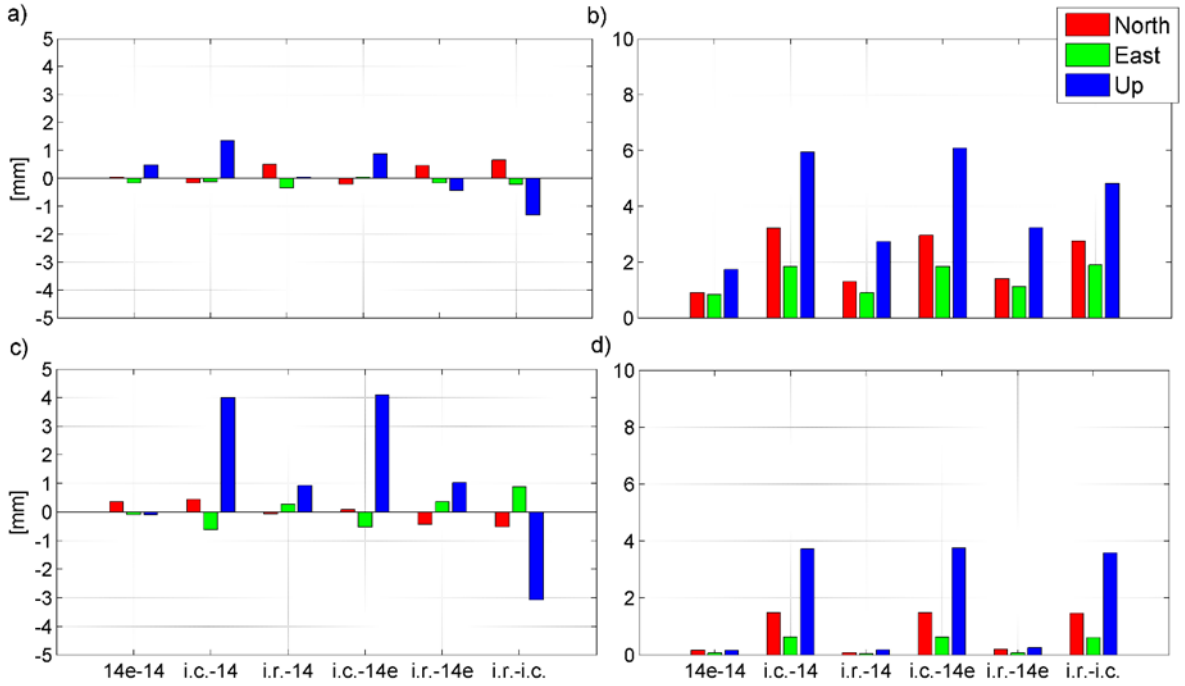

Fig. 7. Mean differences and STD of differences for DILL stations: a) mean from 0.5-hour observation window; b) STD from 0.5-hour observation window; c) mean from daily observation; d) STD from daily observation
Source: own study

In the analyzed cases, switching from a robot-derived model to an individual chamber-derived model generates differences of up to 5 mm for the vertical component (0.5-hour observation window in the case of the DILL station and daily observations in the case of the LDB2 station). The smallest differences were obtained for comparisons of robot-derived models: differences generally do not exceed 2 mm regardless of the station, analyzed variant, or length of the observation session.

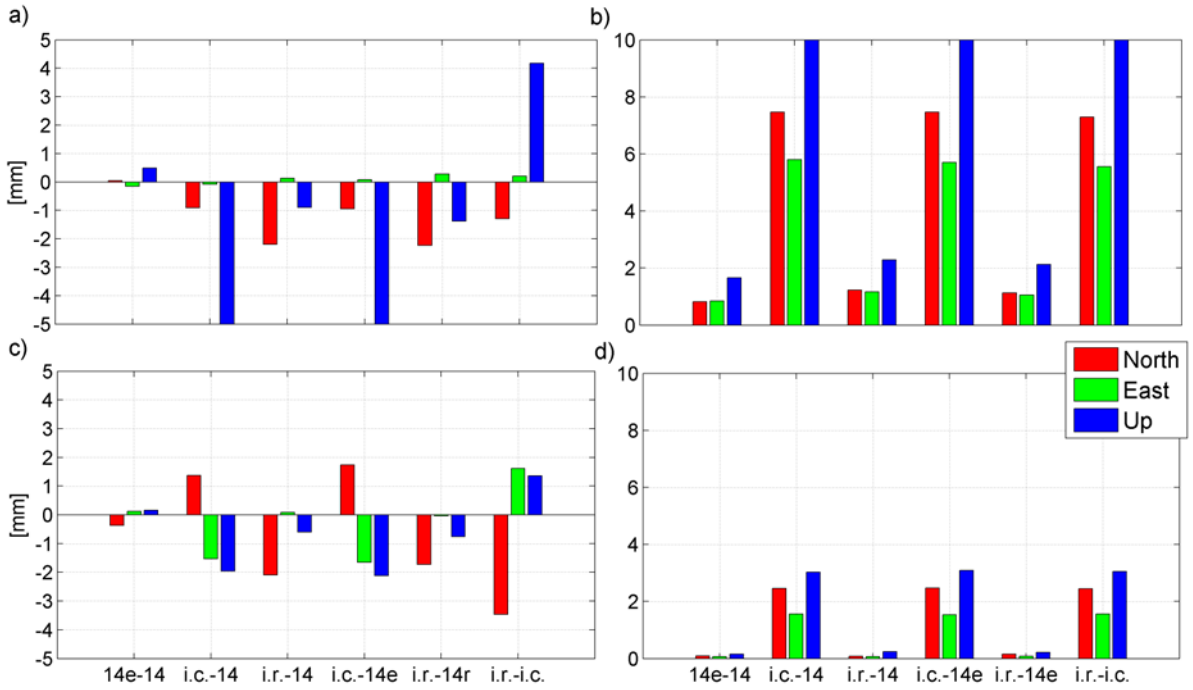

Fig. 8. Mean differences and STD of differences for LDB2 stations: a) mean from 0.5-hour observation window; b) STD from 0.5-hour observation window; c) mean from daily observation; d) STD from daily observation
Source: own study

Analyzing the STD, it was found that the highest values were obtained for comparisons of robot-derived and chamber-derived models. Additionally, in the case of daily observations, as expected, the STD values are significantly smaller than those obtained from 0.5-hour solutions.
It is worth noting that despite the high STD values for both stations, in the case of results obtained from 0.5-hour sessions, the mean differences obtained for these solutions are similar in value to the mean differences obtained from daily solutions.
However, considering the significantly smaller STD values obtained from 24-hour data processing, in the next part of the work, the results for all analyzed stations obtained only from daily solutions are presented - considering them the most reliable.

In the next part of the text, the results for all analyzed stations are presented. An especially significant parameter is the influence of model change on positional components. Fig. 9 shows the mean differences in positional components obtained for each analyzed variant and station. These differences reflect the impact of using various PCC models on the results.

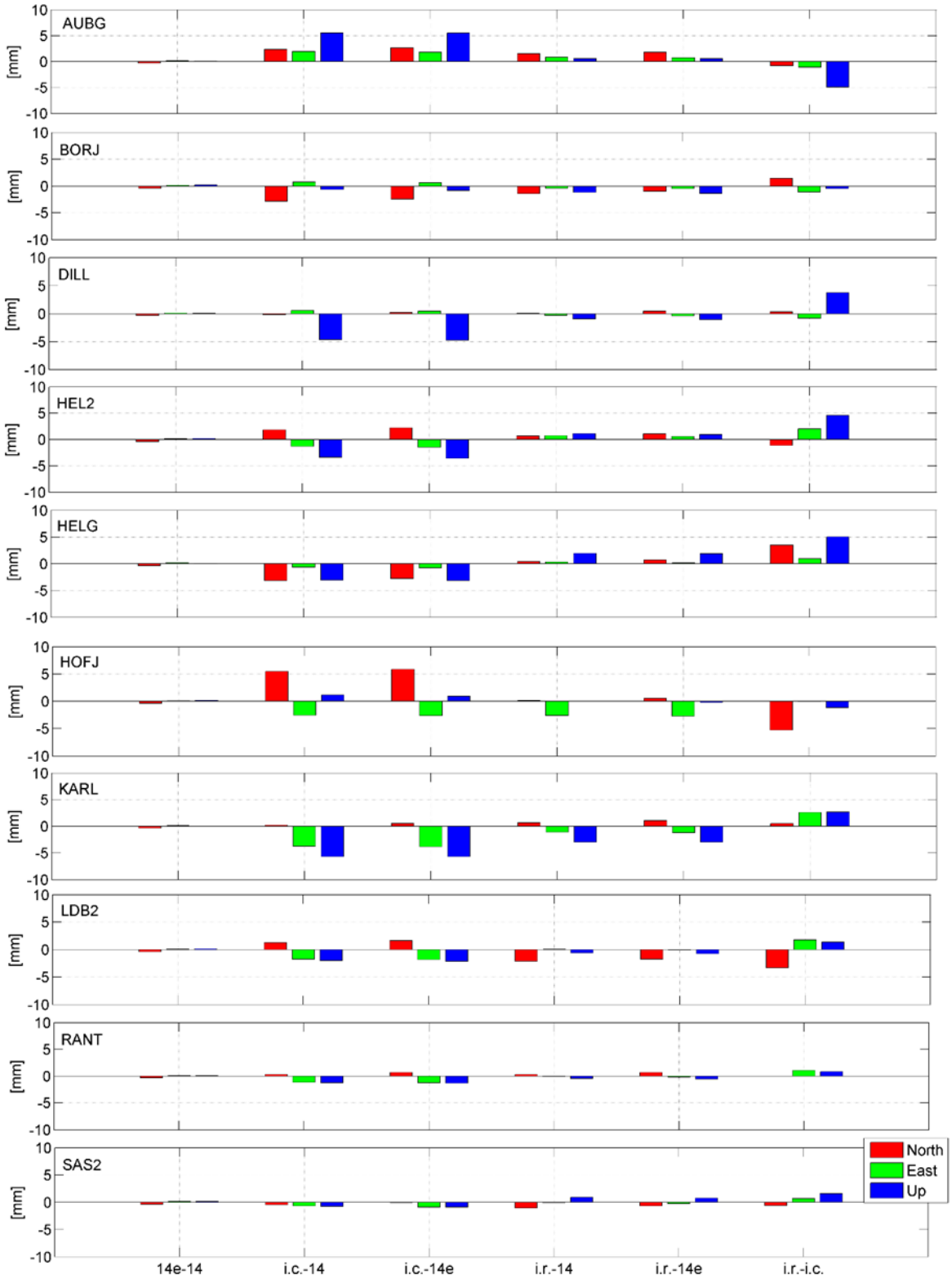

Fig. 9. Mean NEU differences from daily session
Source: own study

In the case of all stations, the conclusions previously drawn are confirmed. Generally, switching from a robot-derived model to an individual chamber-derived

model generates differences of up to 5 mm for the vertical component. The reason lies in the large values of dPCC obtained from comparing these types of PCC models. This applies to almost all stations. The RANT and SAS2 stations are an exception, where the maximum differences in the positional components generally do not exceed 2 mm. The smallest differences in positional components were obtained for comparisons of solutions with robot-derived models: differences generally do not exceed 2 mm regardless of the station, analyzed variant, or length of the observation session. Generally, the differences have a similar magnitude regardless of the station, which may result from using the same type of antenna. An exception is the AUBG station, where the differences have the opposite sign. The detailed values of the mean differences, as well as the absolute mean value of these differences (abs. mean), are presented in Tables 5-7.

Table 5. Mean differences for the North component

STATION	North position component differences [mm]					
	14e-14	i.c.-14	i.c.-14e	i.r.-14	i.r.-14e	i.r.-i.c.
AUBG	-0.3	2.3	2.7	1.5	1.8	-0.9
BORJ	-0.4	-2.9	-2.4	-1.4	-1.0	1.4
DILL	-0.4	-0.2	0.2	0.1	0.5	0.3
HEL2	-0.4	1.8	2.2	0.7	1.1	-1.1
HELG	-0.4	-3.2	-2.8	0.4	0.7	3.5
HOFJ	-0.4	5.5	5.9	0.2	0.6	-5.3
KARL	-0.4	0.2	0.6	0.7	1.1	0.5
LDB2	-0.4	1.3	1.6	-2.1	-1.7	-3.4
RANT	-0.4	0.3	0.7	0.3	0.7	-0.0
SAS2	-0.4	-0.5	-0.1	-1.1	-0.7	-0.6
abs. mean	0.4	1.8	1.9	0.8	1.0	1.7

Source: own study

Table 6. Mean differences for the East component

STATION	East position component differences [mm]					
	14e-14	i.c.-14	i.c.-14e	i.r.-14	i.r.-14e	i.r.-i.c.
AUBG	0.1	1.9	1.8	0.8	0.7	-1.1
BORJ	0.1	0.8	0.6	-0.4	-0.5	-1.2
DILL	0.1	0.5	0.4	-0.3	-0.4	-0.8
HEL2	0.2	-1.3	-1.5	0.7	0.6	2.0
HELG	0.2	-0.6	-0.8	0.3	0.2	0.9
HOFJ	0.1	-2.5	-2.6	-2.6	-2.7	-0.1
KARL	0.1	-3.8	-3.8	-1.1	-1.2	2.6
LDB2	0.1	-1.7	-1.8	0.1	-0.0	1.8
RANT	0.1	-1.2	-1.3	-0.1	-0.2	1.1
SAS2	0.2	-0.7	-0.9	-0.1	-0.3	0.6
abs. mean	0.1	1.5	1.6	0.7	0.7	1.2

Source: own study

Table 7. Mean differences for the Up component

STATION	Up position component differences [mm]					
	14e-14	i.c.-14	i.c.-14e	i.r.-14	i.r.-14e	i.r.-i.c.
AUBG	0.1	5.5	5.5	0.6	0.5	-5.0
BORJ	0.2	-0.7	-0.9	-1.2	-1.4	-0.5
DILL	0.1	-4.7	-4.7	-1.0	-1.0	3.7
HEL2	0.2	-3.4	-3.6	1.2	1.0	4.6
HELG	0.0	-3.1	-3.1	1.9	1.9	5.0
HOFJ	0.2	1.2	1.0	-0.0	-0.2	-1.2
KARL	0.0	-5.7	-5.7	-3.0	-3.0	2.7
LDB2	0.2	-2.0	-2.2	-0.6	-0.8	1.4
RANT	0.1	-1.3	-1.3	-0.4	-0.5	0.8
SAS2	0.1	-0.7	-0.9	0.9	0.7	1.6
abs. mean	0.1	2.8	2.9	1.1	1.1	2.6

Source: own study

Analyzing the results presented in Tables 5-7, it can be observed that on average, differences for the horizontal components do not exceed 2 mm when comparing results obtained using robot-derived and chamber-derived models. For the vertical component, however, they reach up to 3 mm. In the case of comparing results obtained using outdoor calibration models, for horizontal components, the differences do not exceed 1 mm. For the vertical component, they reach a maximum of 1.1 mm.

Summary results for all stations are presented in Fig. 10 in the form of Box Whisker Plots (BWP). These results illustrate the stability of solutions obtained from daily observations. For clarity, only BWP obtained for the vertical component are presented, where the widest spread of results was observed.

Generally, all solutions can be divided into two types: solutions with high stability (all the cases where robot-derived results were compared) and cases with high noise: robot vs chamber-derived results.

Analyzing the results of the specific variant, we can see that the highest stability (small interquartile range, minimum and maximum value, and a number of outliers) is characterized by comparisons 14e-14, i.r.-14, and i.r.-14e. On the other hand, the worst results were obtained for the three remaining solutions where results derived using robot and chamber-derived models were compared.

After analyzing the results for individual stations, we can see that the results are generally very similar. However, we can observe that the worst results were obtained for the HOFJ station (where the widest interquartile range was obtained), while the best results were obtained for the KARL station, where the interquartile range did not exceed 3 mm in any of the variants.

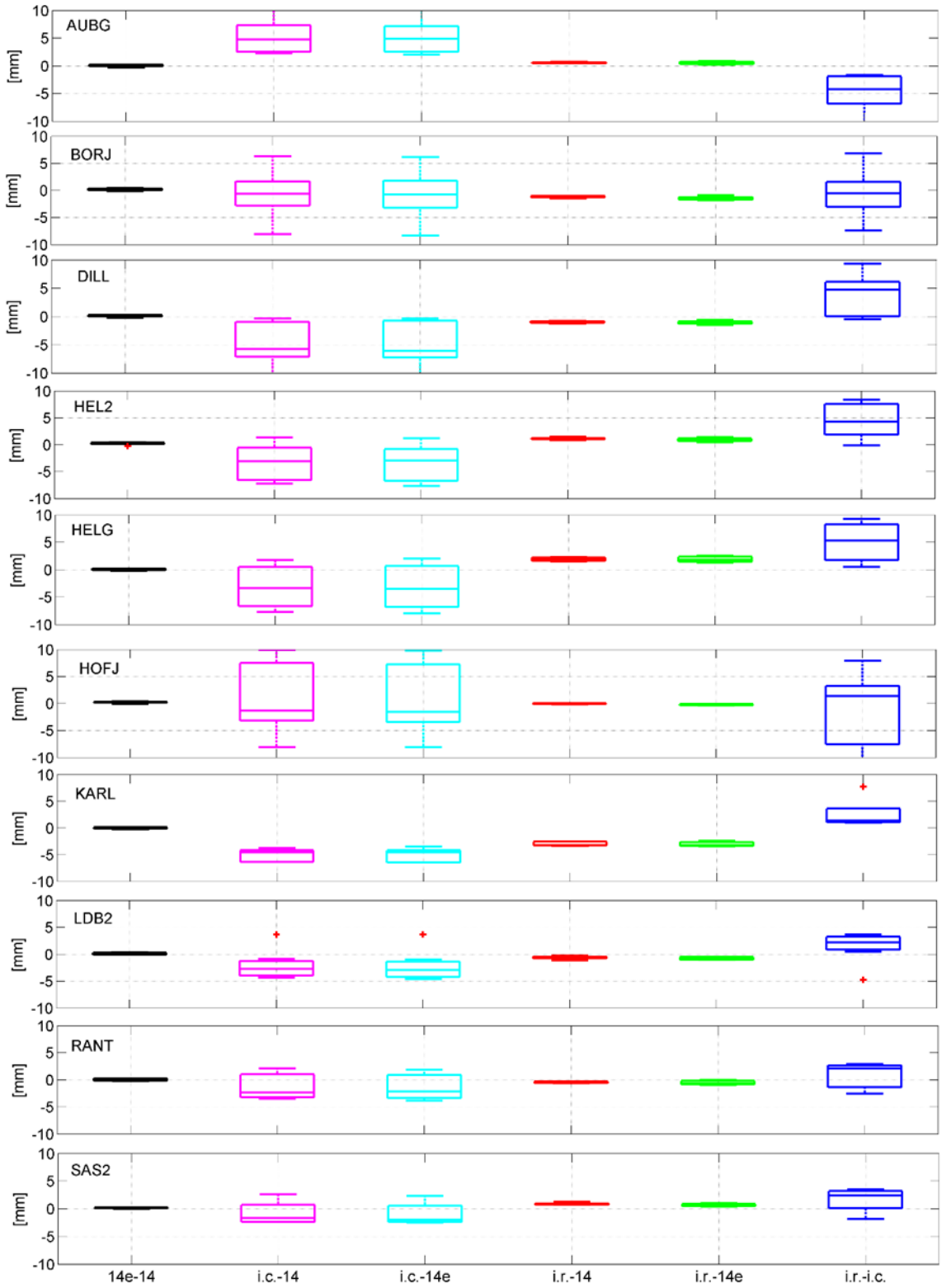

Fig. 10. BWP of Up component differences from daily session
Source: own study

Conclusions

The study presented the differences in position components resulting from using individual or type-mean PCC models. In contrast to previous studies, Galileo-only observations were used in the analyses, and an elevation-only PCC model was introduced. Position components were determined using four PCC models: the igs14_2035.atx model, which contains type-mean calibration results, and two individual antenna models (from the outdoor robot and chamber calibration), as well as the proposed type-mean elevation-only model. Daily GNSS observations from ten selected stations of the European Permanent Network were used for the study. Time series of positions (sub-daily - 30 min and daily) were obtained using Precise Point Positioning technique with the open-source software GAMP.

Generally, it was found that differences for horizontal components generally do not exceed 2 mm in comparison the results obtained using robot-derived and chamber-derived models. However, for the vertical component, they exceed 5 mm for some stations. Meanwhile, in comparison the results obtained using outdoor calibration models, differences for horizontal components mostly do not exceed 1 mm. For the vertical component, they can reach up to 3 mm.

Additionally, it was noted that the solutions where the results obtained using robot-derived models were compared showed the highest stability. And vice versa, the worst results were obtained for the three remaining variants where the results were compared using robot and chamber-derived models. Analyzing the results for individual position components, it was observed that, as expected, the best stability was observed for the horizontal ones. The higher noise was observed for the vertical component.

Acknowledgements

The author acknowledges the EPN providers for the RINEX observation files. We also thank the Centre of Orbit Determination in Europe (CODE) for providing high accurate GNSS products. Special thanks to Zhou et al. for the free sharing of the GAMP software.

References

Baire Q., Bruyninx C., Legrand J., Pottiaux E., Aerts W., Defraigne P., Bergeot N., Chevalier J.M. (2013). Influence of different GPS receiver antenna calibration models on geodetic positioning. GPS Solut., vol. 18, pp. 529–539. https://doi.10.1007/s1029 1-013-0349-1.

Bartolomé J., Maufroid X., Fernandez-Hernandez I., López-Salcedo J., Seco-Granados G. (2014). Overview of Galileo System. Springer, Dordrecht. https://doi.10.1007/978-94-007-1830-2_2.

Bilich A., Mader G. (2010). GNSS absolute antenna calibration at the National Geodetic Survey. In: Proceedings ION GNSS 2010, Institute of Navigation, Portland, Oregon, OR, 21–24 September 2010, pp. 1369–1377.

Dawidowicz K., Krzan G. (2016). Analysis of PCC model dependent periodic signals in GLONASS position time series using Lomb-Scargle periodogram. Acta Geodyn. Geomater., vol. 13, pp. 299–314. https://doi.10.13168/AGG.2016.0012.

Dawidowicz K., Rapiński J., Śmieja M., Wielgosz P., Kwaśniak D., Jarmołowski W., Grzegory T., Tomaszewski D., Janicka J., Gołaszewski P., et al. (2021). Preliminary Results of an Astri/UWM EGNSS Receiver Antenna Calibration Facility. Sensors, vol. 21, no. 4639. https://doi.org/10.3390/s21144639.

Görres B., Campbell J., Becker M., Siemes M. (2006). Absolute calibration of GPS antennas: laboratory results and comparison with field and robot techniques. GPS Solut., vol. 10, pp. 136–145. https://doi.org/10.1007/s10291-005-0015-3.

Hu Z., Zhao Q., Chen G., Wang G., Dai Z., Li T. (2015). First Results of Field Absolute Calibration of the GPS Receiver Antenna at Wuhan University. Sensors, vol. 15, pp. 28717–28731. https://doi.org/10.3390/s151128717.

Krzan G., Dawidowicz K., Wielgosz P. (2020). Antenna phase center correction differences from robot and chamber calibrations: The case study LEIAR25. GPS Solut., vol. 24. https://doi.org/10.1007/s10291-020-0957-5.

Lyard F., Lefevre F., Letellier T., Francis O. (2006). Modelling the global ocean tides: modern insights from FES2004. Ocean Dynamics, vol. 56, pp. 394–415. https://doi.10.1007/s10236-006-0086-x.

Pengfei C., Wei L., Jinzhong B., Hanjiang W., Yanhui C., Hua W. (2011). Performance of precise point positioning (PPP) based on uncombined dual-frequency GPS observables. Survey Rev., vol. 43, pp. 343–350. https://doi.org/10.1179/003962611X13055561708588.

Riddell A., Moore M., Hu G. (2015). Geoscience Australia's GNSS Antenna Calibration Facility: Initial Results. In Proceedings of the International Global Navigation Satellite Systems Society IGNSS Symposium, Gold Coast, Australia, 14–16 July 2015.

Schön S., Kersten T. (2013). On Adequate Comparison of Antenna Phase Center Variations. AGU Fall Meeting, 09-13 December, San Francisco, USA. Washington D.C. American Geophysical Union, 2013. https://doi.org/10.15488/4619.

Tupek A., Zrinjski M., Švaco M., Barković Đ. (2023). GNSS Receiver Antenna Absolute Field Calibration System Development: Testing and Preliminary Results. Remote Sens., vol. 15, no. 4622. https://doi.org/10.3390/rs15184622.

Wang N., Yuan Y., Li Z., Montenbruck O., Tan B. (2016). Determination of differential code biases with multi-GNSS observations. Journal of Geodesy, vol. 90, no. 3, pp. 209-228. https://doi.org/10.1007/s00190-015-0867-4.

Willi D., Lutz S., Brockmann E., Rothacher M. (2020). Absolute field calibration for multi-GNSS receiver antennas at ETH Zurich. GPS Solu., vol. 24, no. 28. https://doi.org/10.1007/s10291-019-0941-0.

Wübbena G., Menge F., Schmitz M., Seeber G., Volksen C. (2000). A New Approach for Field Calibration of Absolute Antenna Phase Centre Variations. Navig. J. Inst. Navig., vol. 44. https://doi.org/10.1002/j.2161-4296.1997.tb02346.x.

Zeimetz P., Kuhlmann H. (2008). On the Accuracy of Absolute GNSS Antenna Calibration and the Conception of a New Anechoic Chamber. In Proceedings of the FIG Working Week 2008, Stockholm, Sweden, 14–19 June.

Zhou F., Dong D., Li W., Jiang X., Wickert J., Schuh H. (2018). GAMP: An open-source software of multi-GNSS precise point positioning using undifferenced and uncombined observations. GPS Solut., vol. 22, no. 33. https://doi.org/10.1007/s10291-018-0699-9.